Electronic Supplementary Material (ESI) for Reaction Chemistry & Engineering.

Supporting Information for:

Production of Jet-Fuel-Range Molecules from Biomass-Derived Mixed Acids

Elnaz Jamalzade,[a,b] Koorosh Kashkooli,[a] Liam Griffin,[a] G. Peter van Walsum[a] and Thomas J. Schwartz*[a]

a. Department of Chemical & Biomedical Engineering and Forest Bioproducts Research Institute, University of Maine, Orono, ME 04469, USA.

b. Department of Chemistry, University of Maine, Orono, ME 04469, USA.

*To whom correspondence should be addressed: thomas.schwartz@maine.edu

Contents

List of Figures and Tables

Experimental Data from the conversion of esterified ethyl hexanoate over $Pd/CeZrO_x$

Table S1. Product distributions from the conversion of esterified ethyl hexanoate.[a]

Products	#C	Initial Selectiviy (%)	Steady State Selectivity (%)
Nonane	9	>1%	>1%
4-Nonanone	9	1%	>1%
Decane	10	1%	>1%
4-Methyl Nonane	10	4%	4%
4-Decanone	10	2%	3%
Undecane	11	34%	7%
3-Methyl Decane	11	>1%	>1%
5-Undecene	11	6%	7%
6-Undecanone	11	>1%	>1%
6-Undecanol	11	11%	40%
Penthyl Benzene	11	6%	1%
6-Methyl Undecane	12	>1%	>1%
1-Hexanone 1-Phenyl	12	>1%	>1%
6-Ethyl Undecane	13	1%	>1%
6-Tridecanone	13	8%	10%
2-Hexyl 1-Octanol	14	>1%	>1%
Tetradecane	14	1%	1%
6-Tetradecanone	14	1%	1%
5-Methyl Tetradecane	15	1%	>1%
Pentadecane	15	1%	>1%
8-Pentadecanone	15	>1%	1%
6-Methyl Pentadecane	16	>1%	>1%
6-Propyl Tridecane	16	>1%	>1%
Hexadecane	16	20%	17%
4-Hexadecanone	16	>1%	>1%
Heptadecane	17	1%	>1%
7-Methyl Hexadecane	17	1%	>1%
7-Octadecene	18	>1%	>1%
Octadecane	18	6%	1%
2-Methyl Octadecane	19	>1%	>1%
Nonadecane	19	1%	2%
2-Methyl Nonadecane	20	1%	>1%
Eicosane	20	>1%	>1%
9-Methyl Nonadecane	20	>1%	>1%
4-Propyl Heptadecane	20	>1%	>1%
2-Methyl Eicosane	21	>1%	>1%
2,6,10,15-Tetramethyl Heptadecane	21	1%	1%
10-Methyl Eicosane	21	>1%	>1%
5-Methyl Heneicosane	22	>1%	>1%
Docosane	22	>1%	>1%
10-Methyl Heneicosane	22	>1%	>1%
9-Hexyl Heptadecane	23	>1%	>1%
6-Methyl Docosane	23	>1%	>1%

Tricosane	23	>1%	>1%
2-Methyl Tricosane	24	1%	>1%
Tetracosane	24	>1%	>1%
Pentacosane	25	>1%	>1%
3-Ethyl 5-(2-ethylbutyl) Octadecane	26	>1%	>1%
7-Hexyl Eicosane	26	>1%	>1%
7-Butyl Docosane	26	>1%	>1%
9-Butyl Docosane	26	>1%	>1%
Hexacosane	26	>1%	>1%
9-Ethyl 9-Hepthyl Octadecane	27	>1%	>1%
Heptacosane	27	>1%	>1%

a. Reaction conditions: 0.25 wt% Pd/CeZrOx at 623 K, 134.9 kPa H_2 pressure, 135.8 kPa total pressure, and WHSV= 0.046 hr^{-1}.

Thermodynamics Calculations

DFT calculation using Gaussian 16[1], the hybrid B3LYP functional[2] with the 6-311g(d,p) basis set was performed to calculate the Gibbs free energy and equilibrium constant for each reaction in suggested reaction pathway.

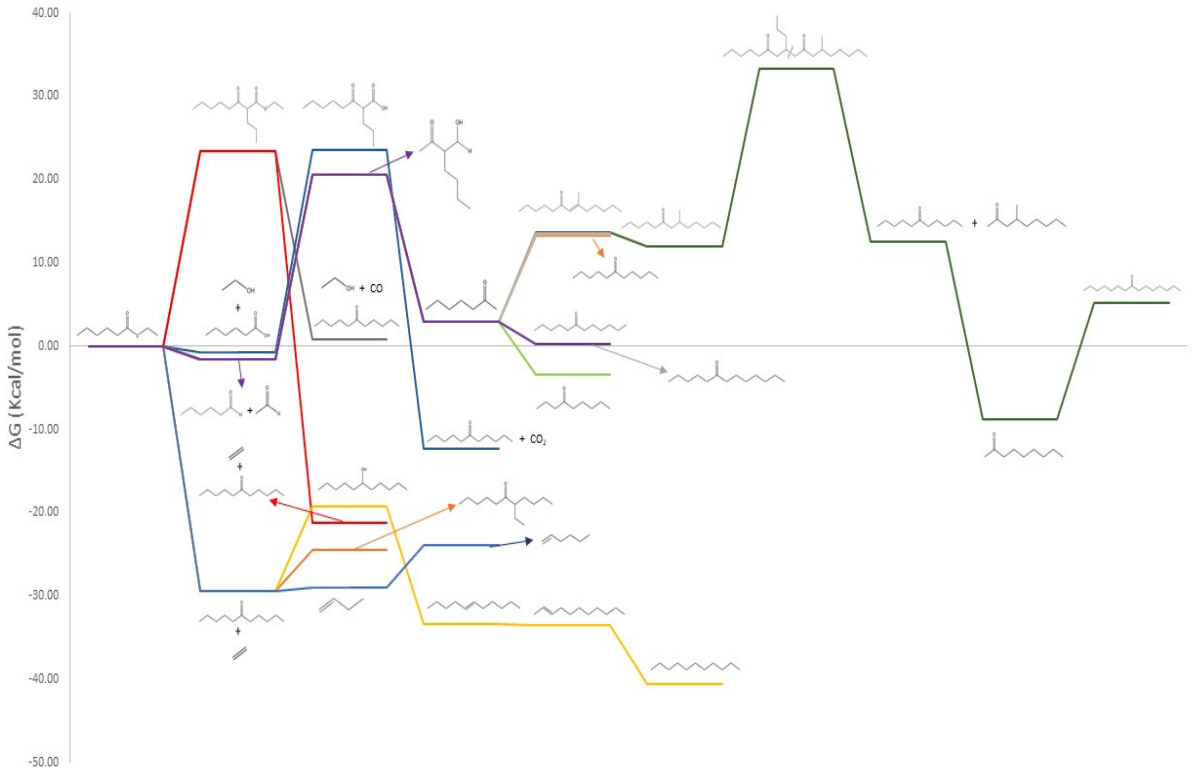

Figure S1. Standard changes of Gibbs free energy (Kcal/mol) for the reactions at 623 K.

Table S2. Calculated K_{eq} for reaction network pathways at 623 K.

Reaction	K_{eq}
A_1	2.03E+10
A_2	1.87E-02
A_3	2.76E-04
A_4	9.58E+04
A_5	1.09
A_6	2.83E+02
A_7	7.37E-01
A_8	1.71E-02
B_1	6.31E-09
B_2	8.26E+07
B_3	4.44E+15
C_1	1.76
C_2	2.99E-09
C_3	4.20E+12
D_1	3.48
D_2	1.80E-08
D_3	1.47E+06
D_4	2.53E-04
D_5	1.69E+02
D_6	1.67E-04
D_7	4.17
D_8	3.31E-08
D_9	1.99E+07
D_{10}	2.98E+07
D_{11}	1.28E-05
D_{12}	2.09E-04
D_{13}	8.54

Catalyst Characterization

BET, BJH

The measured BET surface area is consistent with other reported measurements on $CeZrO_X$ prepared by the same method [3,4]. The BET surface area is not significantly changed by metal loading, showing no changes in the texture of the $CeZrO_X$ after metal deposition.

XRD

Figure S2 shows the XRD pattern obtained for catalyst consisting of 0.25 wt% Pd supported on the ceria-zirconia mixed oxide. All Ceria and ceria-based materials corresponding to cubic-fluorite structure, typical for CeO_2 and showing the main reflections at 28.6°, 33.1°, 47.5°, 56.4°, 59.1°, and 69.5° of 2θ which can be assigned to the (111), (200), (220), (311), (222), and (400) planes. Whereas the pure zirconia shows the monoclinic and tetragonal phases. Here the XRD pattern is mainly showing the CeO_2 cubic-fluorite structure which indicates the solid solution of zirconia dopants and CeO_2 lattice[5]. Also, almost all peaks showed a small shift to higher 2θ compared with pure CeO_2, and this shift is associated with lattice contraction caused by the introduction of smaller Zr^{4+} ions to the CeO_2 lattice[6]. After loading the catalyst with Pd, no change was detected. This can be caused by the well preserved CeO_2 structure in the composite, a small amount of metal loading, and presence of small particles.

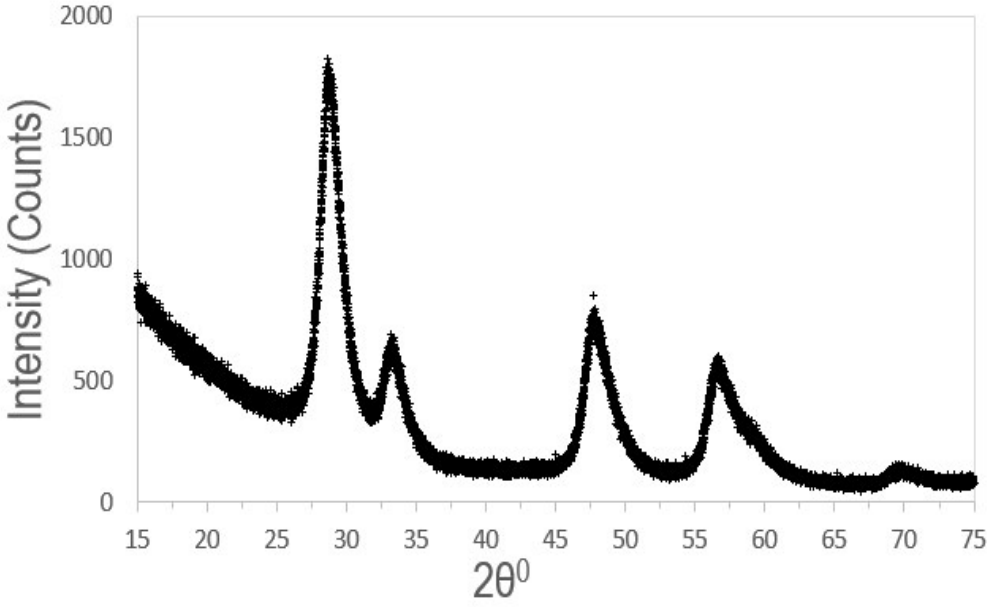

Figure S2. XRD pattern of as-obtained Pd/CeZrOx.

TPD

Temperature-programmed desorption (TPD) of CO_2 was performed using an Altamira AMI-200 instrument equipped with a thermal conductivity detector (TCD). Pure CO_2 was adsorbed at 298 K, after which the catalyst was flushed with He at 298 K to remove excess physisorbed CO_2. The temperature was then ramped at 5 K min^{-1} in flowing He, and the TPD profiles were recorded. The CO_2-TPD profiles of calcined $CeZrO_x$ and MgO-Al_2O_3 catalysts shown in Figure S3. These profiles were integrated to obtain the quantities of basic surface sites. There are 315 µmol/g of base sites on the $CeZrO_x$ catalyst, compared with 352 µmol/g of sites on the MgO-Al_2O_3, an increase of 12 mol%.

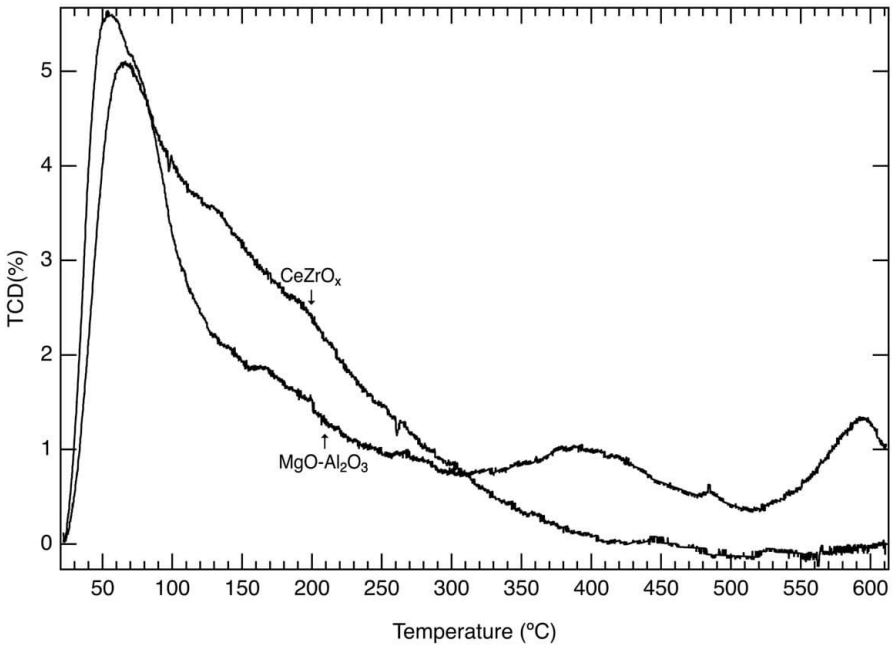

Figure S3. CO_2 desorption profiles from $CeZrO_x$ and MgO-Al_2O_3 catalysts.

References

1 W. C. M. J. Frisch, G. W. Trucks, H. B. Schlegel, G. E. Scuseria, M. A. Robb, J. R. Cheeseman, G. Scalmani, V. Barone, G. A. Petersson, H. Nakatsuji, X. Li, M. Caricato, A. V. Marenich, J. Bloino, B. G. Janesko, R. Gomperts, B. Mennucci, H. P. Hratchian, J. V. , Gaussian 16 Citation, http://gaussian.com/citation/.

2 R. G. P. Chengteh Lee, Weitao Yang, *Phys. Rev. B*.

3 J. C. Serrano-Ruiz, J. Luettich, A. Sepúlveda-Escribano and F. Rodríguez-Reinoso, *J. Catal.*, 2006, **241**, 45–55.

4 R. Klimkiewicz, H. Grabowska and L. Syper, *Kinet. Catal.*, 2003, **44**, 283–286.

5 K. Otsuka, Y. Wang and M. Nakamura, *Appl. Catal. A Gen.*, 1999, **183**, 317–324.

6 E. L. Kunkes, E. I. Gürbüz and J. A. Dumesic, *J. Catal.*, 2009, **266**, 236–249.